RSC Advances

ROYAL SOCIETY OF CHEMISTRY

www.rsc.org/advances

Advances

PAPER

Synthesis and optical properties of emission-tunable PbS/CdS core/shell quantum dots for *in vivo* fluorescence imaging in the second near-infrared window

Yoshikazu Tsukasaki,[a] Masatoshi Morimatsu,[b] Goro Nishimura,[c] Takao Sakata,[d] Hidehiro Yasuda,[d] Akihito Komatsuzaki,[a] Tomonobu M.Watanabe[a,b,e] and Takashi Jin*[a,b,e]

Near-infrared (NIR) fluorescence imaging in wavelengths from 1000 to 1500 nm (2nd-NIR window) is a promising modality for *in vivo* fluorescence imaging because of the deeper tissue penetration with lower tissue scattering of the 2nd-NIR light. For such *in vivo* fluorescence imaging, highly fluorescent probes in the 2nd-NIR wavelength region are needed. Although single-walled carbon nanotubes and Ag_2S quantum dots (QDs) have recently appeared as 2nd-NIR fluorescent probes, their fluorescence brightness is relatively low (quantum yields < 6 %). In this study, we developed a synthetic method for preparing highly fluorescent PbS/CdS core/shell QDs (quantum yields, 17% in water) with narrow band widths (<200 nm) that emit in the 2nd-NIR region. By overcoating of a CdS shell onto a PbS QD core, we could easily control the emission wavelengths of the PbS/CdS QDs in 1000 to 1500 nm. To use the QDs for *in vivo* imaging, we investigated the optical properties of QDs (penetration depth and blurring of fluorescence images in the slices of skin, brain, and heart in mice) in the 2nd-NIR region. We found that the 2nd-NIR fluorescence imaging at ca.1300 nm using the PbS/CdS QDs results in a highest signal to back ground ratio with a low blurring for *in vivo* imaging. To confirm the capabilities of the PbS/CdS QDs for *in vivo* imaging, we conducted fluorescence angiography imaging of a mouse head.

1. Introduction

Near-infrared (NIR) fluorescence imaging is an important modality for the non-invasive visualization of deep tissues at the whole body level, because of the deep penetration and low scattering of NIR light in living tissues.[1-6] This is especially true in the 2nd-NIR window (1000 to 1500 nm), which is expected to offer better spatiotemporal deep tissue imaging due to lower autofluorescence and scattering than that in the 1st-NIR window (700 to 900 nm).[7-9] Although 2nd-NIR emitting fluorescent probes such as single-walled carbon nanotubes[10-23] and Ag_2S quantum dots (QDs)[24-33] have been reported, the fluorescence brightness of these probes is relatively low (quantum yields <

6 %). In this paper, we report highly fluorescent 2nd-NIR emitting probes based on PbS/CdS core/shell QDs[34-41] which emission wavelengths are easily controlled in the 2nd-NIR region. Furthermore, we show the optical properties and utility of the 2nd-NIR emitting PbS/CdS QDs for *in vivo* fluorescence imaging in mice.

In addition to single-walled carbon nanotubes and Ag_2S QDs, PbS QDs should be a candidate as 2nd-NIR fluorescent probes for *in vivo* imaging.[42-47] However, there are a limited number of reports on *in vivo* imaging using 2nd-NIR PbS QDs.[48-50] Recently, we reported the synthesis of water-soluble PbS QDs for 2nd-NIR fluorescence imaging *in vivo*.[50] We demonstrated the utility of the 2nd-NIR PbS QDs for non-invasive fluorescence imaging of a lymph system and breast tumor in mice.[50] Although the emission peaks of PbS QDs are tunable in the range of 1000-1400 nm, the fluorescence quantum yields of PbS QDs significantly decreased with increasing their size. In this work, we synthesized a 2nd-NIR emitting PbS/CdS (core/shell) QDs, where the surface of the PbS core is passivated by a CdS shell, resulting in the increase in fluorescence brightness and stability compared with the PbS QDs previously reported.[50]

To date, PbS/CdS core/shell QDs have been synthesized by using a cation-exchange method,[34,35] where Pb^{2+} cations on the surface of PbS QDs are gradually exchanged with Cd^{2+} cations. In this case, the core size of the PbS decreases with increasing the thickness of the CdS shell. Thus, the emission peak of the resulting PbS/CdS QDs shifts to shorter wavelengths compared with the initial PbS QDs.[34-38] A disadvantage of the cation-

[a] *RIKEN Quantitative Biology Center, 6-2-3 Furuedai, Suita, Osaka 565-0874, Japan. E-mail: tjin@riken.jp*

[b] *Graduate School of Frontier Biosciences, Osaka University, Yamada-oka 2-1, Suita, Osaka 565-0871, Japan.*

[c] *Research Institute for Electronic Science, Hokkaido University, N20W10, Sapporo 001-0020, Japan.*

[d] *Research Center for Ultra-High Voltage Electron Microscopy, Osaka University, Mihogaoka 7-1, Ibaraki, Osaka 567-0047, Japan.*

[e] *Immunology Frontier Research Center, Osaka University, Yamada-oka 1-3, Suita, Osaka 565-0871, Japan.*

exchange method is the long reaction time (1-48 hours)[37] to form a CdS shell in PbS QDs. An alternative for preparing PbS/CdS QDs is a shell-overcoating method,[51] where a CdS shell layer is grown on the surface of a PbS QD core. For example, in the synthesis of 1st-NIR emitting CdSeTe/CdS (core/shell) QDs, a CdS shell is easily formed on the surface of a CdSeTe QD core by thermal decomposition of a Cd-S precursor.[51-53] By the formation of the CdS shell, the fluorescent brightness of CdSeTe/CdS QDs is significantly increased.[51] In this work, we used the shell-overcoating method to prepare highly fluorescent PbS/CdS core/shell QDs as a 2nd-NIR fluorescent probe.

Since the highly PbS/CdS QDs are synthesized using oleylamine as a protecting reagent, the surface of PbS/CdS QDs are hydrophobic and they are insoluble in water. To use the PbS/CdS QDs in aqueous solution, the QDs have to be modified by surface coating. For *in vivo* imaging, small-sized fluorescent QD probes (< ca.10 nm) are desirable to promote the circulation of probes in tissues and their renal clearance.[54] So far, two approaches have been used for the chemical modification of QD surface to be hydrophilic. One method is the encapsulation of QDs with amphiphilic polymers.[55] In principle, this method maintains the fluorescence brightness of the initial QDs, because the QD surface dose not change after the encapsulation. However, the hydrodynamic size of the resulting QDs increases depending on the molecular weights of amphiphilic polymers used for the encapsulation. Another method is the ligand-exchange[55] using small molecules such as hydrophilic thiol compounds. In this case, the size of QDs is not significantly changed when using small molecular-weight ligands. However, the ligand-exchange method often results in a significant decrease in the fluorescence brightness and colloidal stability of QDs.[56] In this study, we have chose the ligand-exchange method to prepare small-sized PbS/CdS QDs with high brightness and water-solubility. We tested several types of thiol compounds such as mercaptoacetic acid (MAA), mercaptoundecanoic acid (MUA), cystein (Cys), and glutathione (GSH) for the surface modification of QDs. Among the thiol compounds, MUA gave highly fluorescent PbS/CdS QDs with a good colloidal stability.

We expected that *in vivo* imaging using highly fluorescent PbS/CdS QDs offers better spatio-temporal deep tissue images in the 2nd-NIR optical window. Modelling studies of QD performance in turbid media containing hemoglobin have suggested that 2nd-NIR fluorescence imaging (at 1320 nm) would improve the signal to noise ratios by a factor of over 10 compared with NIR (at 850 nm) imaging.[8] To appply PbS/CdS QDs as a fluorescent probes in the 2nd-NIR window, we systematically investigated the optical properties of PbS/CdS QDs in the tissues such as skin, brain, and heart of mice. Moreover, we conducted fluorescence angiography of a mouse head to demonstrate the capabilities of PbS/CdS QDs for deep tissue imaging in the 2nd-NIR window.

2. Experimental

2.1 Materials

Lead (II) chloride, oleylamine, and oleic acid were purchased from Wako Pure Chemical Industries. Hexamethyldisilathiane and tributylphosphine (TBP) were purchased from TCI Chemicals. Mercaptoundecanoic acid (MUA), 1-ethyl-3-(3-dimethylaminopropyl) carbodiimide hydrochloride (EDC) and bovine serum albumin (BSA) was purchased from Sigma-Aldrich. Cadmium 2,4-pentanedionate (98%) was purchased from Alfa Aesar. Selenium (powder, 99.999%) and dimethylcadmium (10 wt% in hexane) was purchased from Strem Chemicals.

Tetrahydrofuran, Diethylzinc (1M hexane solution), potassium *t*-butoxide, mercaptoacetic acid (MAA), *L*-cystein (Cys), and glutathione (GSH) were Wako Pure Chemical Industries. Other chemicals used were of analytical grade reagents.

2.2 Synthesis of PbS and PbS/CdS QDs

Lead (II) chloride (278 mg) was dissolved in a mixture of 5 mL of oleylamine and 1 mL of oleic acid in a three-necked flask at room temperature. The solution was heated to 100-150 ^{o}C under an argon atmosphere. To this solution, 0.5 mL of a sulfur precursor solution (0.5 mL of hexamethyldisilathiane and 9.5 mL of TBP) was dropwisely added under vigorous stirring. The formation of PbS QDs was monitored by observing their emission spectra, which shifted to longer wavelengths with increasing the amount of the sulfur precursor solution. The reaction temperature was set to 100 ^{o}C, 125 ^{o}C, and 150 ^{o}C for preparing 1000, 1200 and 1400 nm emitting PbS QDs, respectively. When the desired emission peak of the PbS QDs was obtained, the solution was quickly cooled to 60 ^{o}C. Then, methanol was added to the solution to precipitate the PbS QDs. The PbS QD precipitates were dissolved in a mixture of 2 mL of oleylamine and 20 mL of toluene at room temperature. The solution was heated to 90 ^{o}C, and 0.25-0.5 mL of a Cd-S precursor solution (2.5 mL of dimethylcadmium solution + 0.5 mL of hexamethyldisilathiane + 7.5 mL TBP) was added dropwisely. By measuring the fluorescence spectra of the solution, the shell formation of CdS was monitored. When the desired emission peak of the PbS/CdS QDs was obtained, the solution was cooled to 50 ^{o}C. Then, ethanol was added to the solution to precipitate the PbS/CdS QDs, and the QD precipitations were dissolved in tetrahydrofuran. By controlling the amounts of a Cd-S precursor solution during the shell formation, PbS/CdS QDs with emission peaks of 1100, 1300 and 1500 nm were obtained from the PbS QDs with emission peaks of 1000, 1200 and 1400 nm, respectively.

2.3 Synthesis of CdSe/ZnS and CdSeTe/CdS QDs

Visible (VIS)-emitting CdSe/ZnS QDs[52] （520 nm emission） and 1st-NIR emitting CdSeTe/CdS QDs[51,53] (720 nm emission) were synthesized as described previously.

2.4 Surface modification of QDs

To 1 mL of the tetrahydrofuran solution of PbS/CdS QDs (1 μM), 1 mL of a MAA or MUA solution (50 mg/mL in tetrahydrofuran) was added under stirring. To this solution, 0.5 mL of aqueous solution (50 mg/mL of potassium *t*-butoxide) was added to precipitate the MAA or MUA-coated PbS/CdS QDs. The PbS/CdS QD precipitates were separated by centrifugation and dissolved in water. An aqueous solution of PbS/CdS QDs was passed through a 0.22 μm membrane filter and centrifuged at 15,000 g for 5 min to remove aggregated PbS/CdS QDs. The surface modification of CdSe/ZnS and CdSeTe/CdS QDs were performed using the same method described above. The surface modification of QDs with Cys and GSH were performed by a previously reported method.[51]

2.5 Conjugation of BSA to QDs.

To 1 mL of an aqueous solution of MUA-coated QDs (1 μM, PBS buffer, pH 7.4), 10 μL of an aqueous solution (1 mM) of EDC was added under stirring. After 30 min, 100 μL of a BSA

solution (1 mM in PBS buffer, pH 7.4) was added to the solution, and the mixture was incubated for 1 hour at room temperature. Unconjugated BSA and EDC were removed using an ultrafiltration membrane that had a 100 kDa molecular weight cut-off (GE Healthcare) and PBS buffer (pH 7.4).

2.6 Characterization of PbS/CdS QDs.

Fluorescence spectra of PbS/CdS QDs were measured by a NanoLog spectrometer system with an InGaAs photodiode array (Symphony; HORIBA) at an excitation of 488 nm. Absorption spectra of QDs were measured with a V-670 spectrophotometer (JASCO Corporation). The hydrodynamic size of PbS/CdS QDs was estimated from dynamic light scattering using the Zetasizer Nano-ZS (Malvern) and a 633 He/Ne laser. Powder X-ray diffraction (XRD) patterns were obtained using the D2 PHASER diffractometer (BRUKER), which employs a Cu Kα (λ = 1.5406 Å) Transmission electron micrographs of PbS/CdS QDs were taken by using the Hitachi HF2000 (Hitachi High-technologies) at 200 kV. Samples were prepared by dropping 2 μL of solution onto a carbon-coated copper grid and stood overnight to evaporate the solvent. Inductively coupled plasma mass spectrometry (ICP- MS) spectra were obtained using the Agilent 7700 (Agilent technologies) set at the helium collision mode. All samples were dissolved in 5% HNO_3 and mineralized. Instruments were tuned using 1 μg/L of Li, Mg, Co, Y, Ce and Tl as the standards. Fluorescence quantum yields (QYs) of PbS/CdS QDs with emission peaks of 1100, 1300 and 1500 nm were estimated relatively using standard PbS QDs, which had an emission peak of 1000 nm. Fluorescence QY of this PbS QDs was determined to be 0.6 by an absolute quantum yield measurement systems (C10027; Hamamatsu photonics). By comparing the fluorescence intensities of the standard PbS QDs and PbS/CdS QDs with OD = 0.1 at 488 nm, fluorescence QYs of the PbS/CdS QDs were calculated. Molar extinction coefficients (ε) of PbS/CdS QDs were determined with the aid of fluorescence correlation spectroscopy (FCS) as follows. The surface of the PbS/CdS QDs was coated with FITC-labeled polyethyleneimine (MW 25000), and the concentration of the QDs in water was measured by FCS using a Rh6G standard solution (10^{-8} M). The molar extinction coefficient, ε, for PbS/CdS QDs in water was determined from the Lambert-Beer relationship (absorbance = $\varepsilon c l$, where c is the concentration of the solution and l is the path length) as 6.3×10^5, 16.6×10^5 and 22.4×10^5 M^{-1} cm^{-1} for PbS/CdS with emission peaks of 1100, 1300, and 1500 nm, respectively, at an absorption wavelength of 488 nm.

2.7 VIS, 1st-NIR and 2nd-NIR imaging system

The imaging system was based on the Macro Zoom System with zoom function from 0.63× to 6.3× (MVX; Olympus). The optics was optimized in the VIS, 1st-NIR, and 2nd-NIR windows with custom designed objective and tube lenses for *in vivo* fluorescence imaging. GFP and Cy5.5 filter sets (Semrock) were used for the VIS and 1st-NIR imaging, respectively. A filter set consisting of an excitation filter for the 785 nm laser, dichroic mirror to reflect the 785 nm laser and transmit over 800 nm, and long-pass emission filter with the cut-off wavelength at 800 nm, was used for 2nd-NIR imaging. Emission filters of 1100 ± 25 nm, 1300 ± 25 nm, and 1500 ± 25 nm placed after the filter set were used for the imaging. A Xe lamp was used as the excitation light source at 482 nm for VIS imaging. 670 nm and 785 nm laser diodes (BWF1 series; B&W TEK) were used as the excitation light for the 1st-NIR and 2nd-NIR imaging, respectively. Maximum excitation powers on the sample stage were 5.0

mW/cm^2 at 482 nm excitation, 25.1 mW/cm^2 at 670 nm excitation, and 25.5 mW/cm^2 at 785 nm excitation at 0.63× magnification. A Si EM camera (iXon3, Andor) was used for VIS and 1st-NIR imaging, and an InGaAs CMOS camera (C10633-34; Hamamatsu photonics) for 2nd-NIR imaging. Device control and data acquisition were performed by IQ2 (Andor) and HCImage (Hamamatsu photonics) software and a LabVIEW program (National Instruments).

2.8 Optical property measurements for tissue slices

A solution of 15 μm porous beads (SOUCE 15ISO; GE healthcare) was dried and exchanged into 2-propanol. A chloroform solution of QDs (520, 720, 1100, 1300 and 1500 nm emission) was added to the porous beads solution. After incubation for one hour, the porous bead solution was centrifuged, and the solvent was gradually exchanged with 10 mg/mL BSA solution in PBS (pH 7.4). Skin, brain and heart were extracted from HOS:HR-1 mice (Hoshino Laboratory animals). Each specimen was enclosed with two glass cover slips for autofluorescence measurements. Brain and heart slices of various thicknesses were made by a microslicer (DTK-1000; Dosaka EM) and placed between the glass cover slips with or without the solution of 15 μm porous beads. Microscopic images were taken at 6.3× magnification. For quantitative comparisons of autofluorescence between VIS, 1st-NIR and 2nd-NIR imaging, image intensities were corrected for photon counts per unit excitation power and unit bandwidth of the emission filter. Optical property analysis was performed using G-track (G-angstrom), G-count (G-angstrom), image J, Origin (OriginLab) software and a program made with LabVIEW.

2.9 Fluorescence angiography of a mouse head

Mice were anesthetized on a microscope stage. Mouse heads were observed at 0.63× magnification. For fluorescence angiography, a 150 μL of the mixture of BSA-coated QDs solutions (ca.1 μM) was injected into a mouse tail vein. The brightness of fluorescence images of a mouse head for the BSA-coated QDs (520, 720, and 1300 nm emission) were normalized by the peak intensities of the QD fluorescence.

All animal experiments were performed in compliance with the National Institutes of Health Guidelines for Care and Use of Laboratory Animals and were approves by the Osaka University Animal Care and Use Committee.

3. Results and discussion

3.1 Synthesis and characterization of PbS/CdS QDs

To prepare PbS/CdS core/shell QDs, a cation-exchange method is widely used to make a CdS shell. In this method, a CdS shell is grown by exchange of Pb^{2+} ions with Cd^{2+} ions at the surface of PbS core QDs. The resulting PbS/CdS QDs emit at shorter
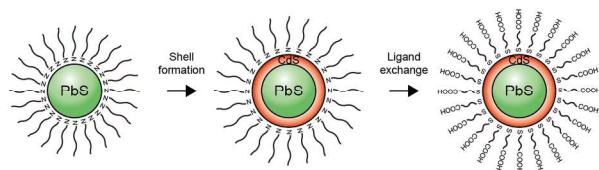
Fig.1 Schematic presentation of the synthesis of MUA-coated PbS/CdS QDs. A CdS shell onto a PbS core is formed using a Cd-S precursor of dimethylcadmium and hexamethyldisilathiane. Ligand-exchange with MUA is performed to obtain water-soluble PbS/CdS QDs.
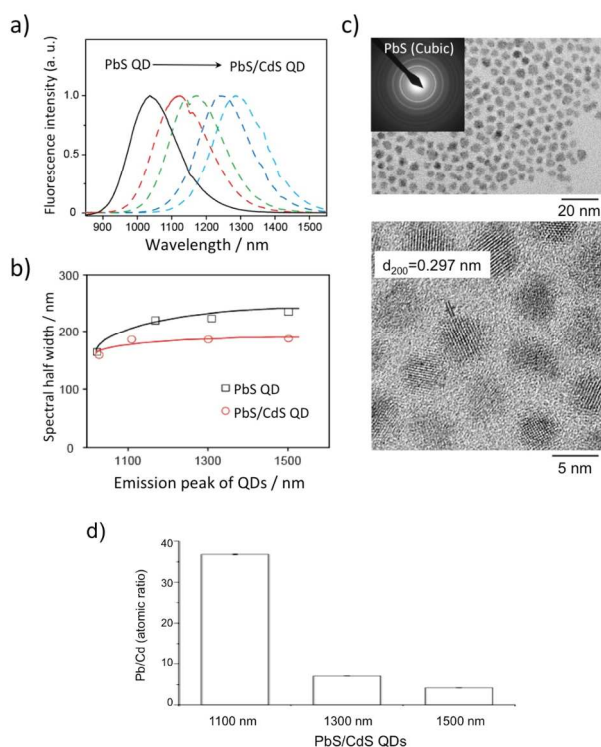
Fig.2 a) Spectral changes of PbS QDs upon formation of the CdS shell. A black line shows the fluorescence spectrum of the PbS QDs before the shell formation. Dotted red, green, dark blue and light blue lines show the fluorescence spectra of PbS/CdS QDs with increasing their size. b) Spectral half widths of PbS and PbS/CdS QDs in chloroform. Black and red plots show spectral half widths versus emission peaks of PbS and PbS/CdS QDs, respectively. c) TEM images of PbS/CdS QDs with an emission peak of 1300 nm. d) Elemental analysis of PbS/CdS QDs with 1100, 1300 and 1500 nm emission, obtained from ICP mass spectroscopy.

wavelengths compared with that of the initial PbS QDs.[34-41] A disadvantage of the cation-exchange method is the long reaction time (1-48 hours) to form a CdS shell.[37] As an alternative for preparing PbS/CdS QDs is a shell-overcoating method[57,58] where
5 a CdS shell is formed at the surface of a PbS QD by the pyrolysis of a Cd-S precursor such as a mixture of dimethyl cadmium and hexamethyldisialthiane (Fig.1). In this case, the emission peak of the resulting PbS/CdS QDs shifts to longer wavelengths with increasing the amount of the Cd-S precursor (Fig.2a). Compared
10 with the cation-exchange method, shell-overcoating method is facile and rapid: the shell formation is completed within one hour. The spectral width of the resulting PbS/CdS QDs is almost constant (< 200 nm) in the emission wavelength from 1100 to 1300 nm (Fig.2b). In contrast, the spectral width of PbS QDs
15 increases with increasing the emission wavelengths, and the width is approximately 10-30% larger than those of PbS/CdS QDs. The crystallinity of the PbS/CdS QDs is confirmed by transmission electron microscopy (TEM) images (Fig.2c). The TEM image of the PbS/CdS QDs (1300 nm emission) shows that
20 the QDs have spherical shapes (ca. 5 nm in diameter) with lattice fringes, confirming the highly crystalline nature with a cubic structure (Fig.2c). However, the structure of a CdS shell in the PbS/CdS QDs was not observed from the TEM image. This may be due to a thin layer of the CdS shell less than ca. 1 nm. Similar
25 observation has been reported for the PbS/CdS QDs with thin CdS shells prepared by using a cation-exchange method.[37] To confirm the formation of a CdS shell, we measured X-ray diffraction (XRD) pattern and ICP mass spectra for the PbS/CdS
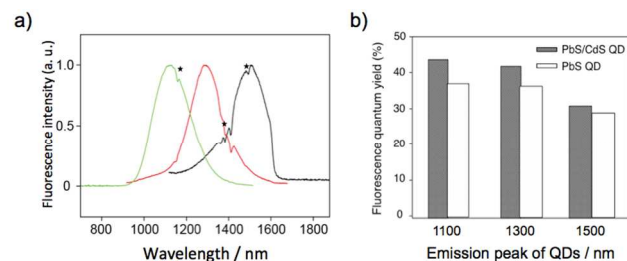
Fig.3 (a) Fluorescence spectra of PbS/CdS QDs emitting at 1100 nm, 1300 nm and 1500 nm in chloroform. Asterisk shows the fluorescence absorption by the solvent, chloroform. (b) Fluorescence QYs of the three types PbS QDs and PbS/CdS QDs in chloroform.

QDs (Fig. S1). XRD pattern of the PbS/CdS QDs (1300 nm
30 emission) was slightly different from that of PbS QDs due to the CdS shell on the PbS QDs (Fig.S1a). Elemental analysis of the PbS/CdS QDs by ICP mass spectroscopy showed the a clear evidence that the CdS shell forms on the surface of PbS QDs (Fig S1b): the atomic ratios of Pb/Cd are measured to be 81, 7.1, and
35 4.2 for the PbS/CdS QDs with 1100, 1300, and 1500 nm emission, respectively (Fig.2d).

In addition to the emission tunability of PbS/CdS QDs in the 2nd-NIR window (Fig.1a), these QDs have high fluorescence QYs. For *in vivo* tissue imaging, fluorescence probes with higher
40 QYs are desirable to obtain clear images with higher signal to background ratios, where the background fluorescence signals usually arise from autofluorescence from tissues. We measured the QYs of PbS/CdS QDs with the emission peak of 1100 nm, 1300 nm, and 1500 nm (Fig. 3a), which were prepared from the
45 initial PbS QDs with the emission peak of 1000 nm, 1200 nm, and 1300 nm, respectively. Fig.3b shows the fluorescence QYs of the PbS/CdS QDs and PbS QDs. The QYs of PbS/CdS QDs are 0.3-0.45 in chloroform, and their values are higher than that of PbS QDs by a factor of 10-18 %.
50

3.2 Water-solubilization of PbS/CdS QDs by surface modification

The highly fluorescent PbS/CdS QDs prepared in organic phases
55 are coating with oleylamine.[35-41] To use the PbS/CdS QDs in aqueous phase, surface modification should be be performed to make the QD surface hydrophilic. We used a ligand-exchange method to prepare a small-sized water-soluble PbS/CdS QDs. We tested four thiol compounds, MAA, MUA, Cys, and GSH for the
60 ligand exchange. In the case of MAA, Cys, and GSH, the resulting water-soluble PbS/CdS QDs aggregated in aqueous solution (10 mM PBS, pH=7.4) within 1-3 days after the surface modification. In contrast, the ligand exchange using MUA resulted in highly stable water-solube PbS/CdS QDs with a high
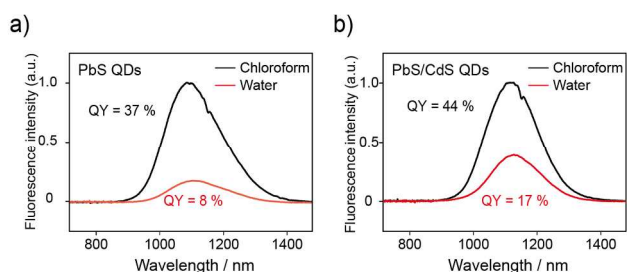
Fig.4 Fluorescence spectra of PbS QDs (a) and PbS/CdS QDs (b) emitting at 1100 nm before and after the ligand-exchange with MUA. The spectra were obtained by the excitation of 488 nm.
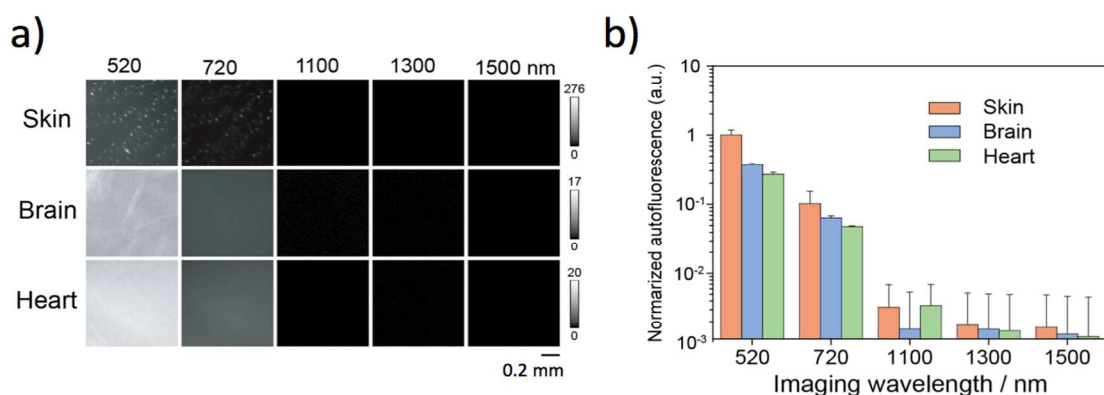
Fig.5 (a) Autofluorescence images from tissues. VIS, 1st-NIR, and 2nd-NIR autofluorescence were observed at an excitation of 482 nm, 670 nm, and 785 nm, respectively. (b) Quantitative comparison of autofluorescence from tissues. Red, blue and green boxes indicate results for skin, brain and heart samples, respectively.

brightness in PBS solution. MUA-coated PbS/CdS QDs did not aggregate in the PBS solution over one month.

Fig. 4 shows the fluorescence spectra of PbS QDs and PbS/CdS QDs (1100 nm emission) before and after the ligand
5 exchange with MUA. The quantum yield (QY) of the MUA-coated PbS/CdS QDs (QY, 17 % in PBS) was much higher than that of MUA-coated PbS QDs (QY, 8 % in PBS). For the MUA-PbS/CdS QDs with 1300 and 1500 nm emissions, we could not determine the QY values in PBS, because of the strong
10 absorption of their fluorescence by water medium. The

hydrodynamic diameter of the MUA-PbS/CdS QDs was determined to be 4.5 nm, 7.7 nm and 10. 5 nm for the QDs emitting at 1100 nm, 1300 and 1500 nm, respectively (Fig S2).

3.3 Optical properties of tissues and PbS/CdS QDs in the 2nd-
15 **NIR window**

2nd-NIR light (1000-1500 nm) can penetrate biological tissues more deeply than VIS light (400-700 nm) and 1st-NIR light (700-1000 nm), because of the lower scattering and absorption at longer wavelengths in the tissues.[7,8] However, there are no
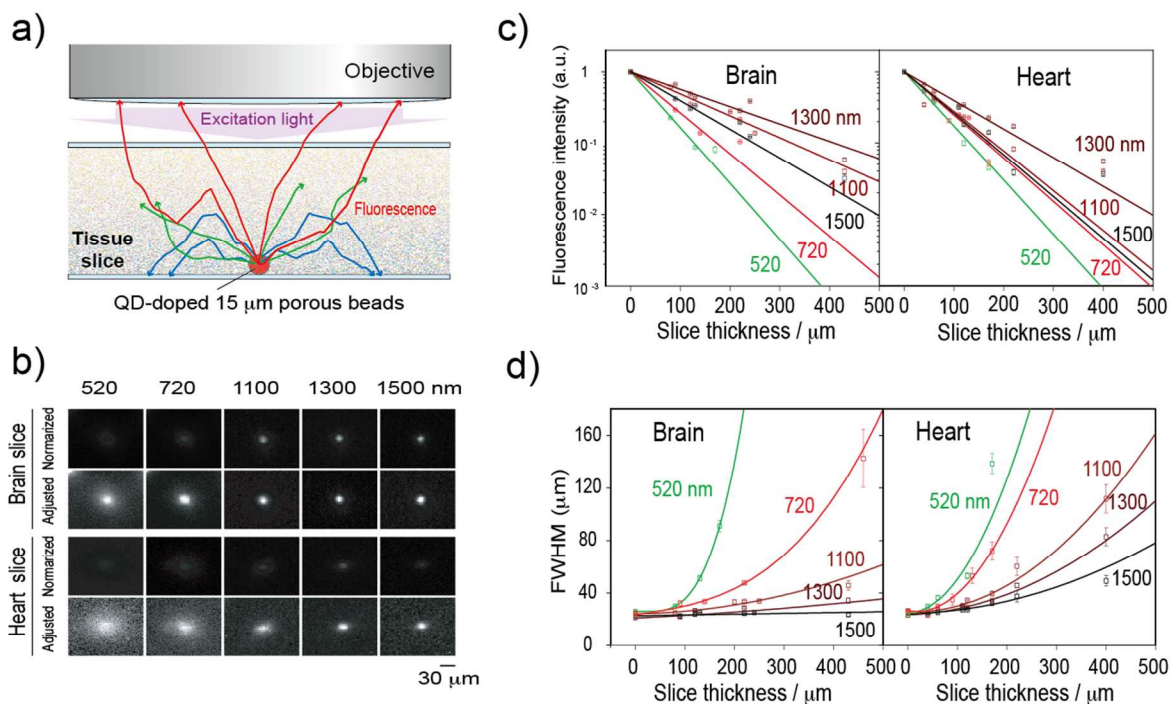
Fig.6 (a) Schematic representation of an imaging experiment with tissue slices. A tissue slice was sandwiched between two glass cover slips (top and bottom glass). The red particle represents a QD-doped porous bead (15 μm in diameter), and the purple arrow represents the excitation light. Red, green and blue traces show transmitted, absorbed and back scattered light emitted from the bead, respectively. (b) Microscopic images of the fluorescence of QD-doped porous beads (15 μm in diameter) and their passage through tissue. Slice thicknesses of the brain and heart were 100 and 200 μm, respectively. Normalized images show the fluorescent intensities normalized against the intensities in the absence of tissue slices. Adjusted images show the fluorescent intensities normalized to the peak to peak intensity. (c) Fluorescence intensities of a QD-doped porous bead versus slice thickness in the brain and heart. Green, red, brown, dark brown and black indicate fluorescence intensities observed at 520, 720, 1100, 1300 and 1500 nm, respectively. Slice thickness = 0 describes when the beads are located at the top glass. (d) Full width at half maximum (FWHM) of the fluorescence spots in (b) versus slice thickness in brain and heart slices. The solid lines are curves of the spline fits.

systematic data on the relationship between wavelengths of excitation/emission light and imaging resolution in biological tissues. We therefore conducted a quantitative analysis of optical properties of VIS (CdSe/ZnS; 520 nm), 1st-NIR (CdSeTe/CdS;

5 720 nm) and 2nd-NIR QDs (PbS/CdS; 1100, 1300, and 1500 nm) in tissues with a newly designed up-right microscope system (Fig S3). We first measured the autofluorescence of mouse tissues such as skin, brain and heart excitations of 482 nm for VIS, 670 nm for 1st-NIR and 785 nm for 2nd-NIR imaging (Fig.

10 5a). Autofluorescence due to endogenous chromophores in tissues results in generating background noise to reduce the detection sensitivity.[1,7] In the 2nd-NIR region, there are no significant autofluorescence compared with the VIS and 1st-NIR region (Fig. 5b).

15 To quantify the penetration ability and imaging resolution in tissues, we observed the fluorescence spots of porous beads (15 μm in diameter) doped with VIS, 1st-NIR and 2nd-NIR QDs in brain and heart slices (Fig. 6a). Fluorescence images of the beads show that the 2nd-NIR images, especially in the 1300 nm

20 window, are brightest for all tissues (Fig. 6b,c). Furthermore, the images show that the effect of blurring in relation to the imaging resolution decreases with an increase in the imaging wavelength owing to less light scattering by the tissues. The effects of slice thickness of brain and heart tissues on the normalized intensity

25 and full width at half maximum (FWHM) of the fluorescence spots are summarized in Fig. 6c and 6d. The change in the fluorescence intensity is well fitted by an exponential decay curve. The penetration depth, which is defined as $1/\mu_t$ (μ_t: attenuation coefficient),[59] was estimated from the slope and largest at 1300

30 nm, about 1.9-3.2 times that from conventional NIR imaging (Table S1). The effect of thickness on light attenuation through the tissue specimen could be reproduced by a Monte Carlo simulation using estimated optical parameters from integrating sphere measurements (Fig S4). The FWHM increases with

35 thicker slices or shorter wavelengths, showing that the imaging resolution in deep tissue can be significantly improved by increasing the light wavelength. To understand how autofluorescence affects the detection sensitivity of 2nd-NIR imaging, we quantified the signal to background ratios, which are

40 an important factor for determining the detection sensitivity of *in vivo* optical imaging. As thickness of the tissue slice increases, the peak intensities of the signal should decrease due to light blurring and attenuation. We found that at a heart slice thickness of 120 μm, the signal to background ratio of 2nd-NIR imaging (at

45 1300 nm) can be improved 76 times compared to that of 1st-NIR fluorescence (at 720 nm) imaging (Fig. S5).

3.4 Fluorescence angiography of a mouse head

To demonstrate the capability of 2nd-NIR imaging *in vivo*, we

50 performed fluorescence angiography[60] for a mouse head using bovine serum albumin (BSA) conjugated VIS, 1st-NIR, and 2nd-NIR QDs. For BSA-conjugated PbS/CdS QDs, we confirmed that their cytotoxicity is very low at the concentration of less than 100 nM (Fig. S6). The mixture of each QD solution was injected into

55 a mouse tail vein, and the angiography images were taken at the VIS, 1st-NIR, and 2nd-NIR regions. Autofluorescence of the mouse body dramatically decreased in the angiography of 2nd-NIR images compared with that of the VIS and 1st-NIR images. Blood vessels show a clearer image in the 2nd-NIR region (Fig.

60 7) due to higher penetration of the 2nd-NIR light with lower autofluorescence in the tissue. It should be noted that the spatial-resolution of the fluorescence image of the blood vessels is improved by increasing the imaging wavelength, which also increases the signal to background ratio in the 2nd-NIR image
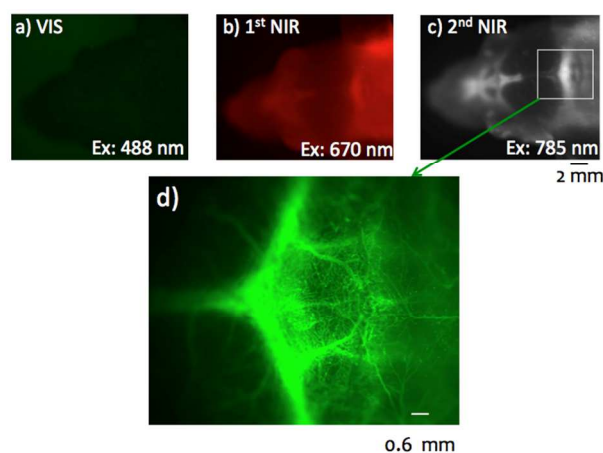
Fig.7 Fluorescence angiography of a mouse head. The images (a-c) show its Vis (520 nm), 1st-NMR (720 nm), and 2nd-NIR (1300 nm) fluorescence angiographies, where excitation wavelengths are set to 488 nm, 670 nm, and 785 nm, respectively. The image (d) shows the magnification of a square area in (c).

65 compared with VIS or 1st-NIR images. The difference in the signal to background ratio, however, was less than that seen in the tissue slice measurements, indicating that the multiple scattering of light in biological tissues contributes to the background fluorescence signal.

70 ## 4. Conclusions

In summary, we have presented the synthesis and optical properties of PbS/CdS QDs prepared by using a shell-overcoating method. Compared with a cation-exchange method, the shell-overcoating method is facile to prepare the PbS/CdS QDs that

75 emit at wavelengths in the 2nd-NIR window. Using a ligand-exchange with MUA, we could obtain highly fluorescent, small-sized PbS/CdS QDs than can be used for non-invasive 2nd-NIR fluorescence imaging. MUA-coated PbS/CdS QDs have sufficient sensitivity for deep tissue imaging and show great

80 promise for the non-invasive imaging of tissues *in vivo*. Although the PbS/CdS QDs contain heavy metals, their cytotoxicity is very low at the QD concentrations used. Moreover, compared with single-walled carbon nanotubes and Ag_2S QDs, PbS/CdS QDs are highly fluorescent (17 %) and their emission is size-tunable.

85 This is a tremendous advantage when studying biological systems, because it is essential to simultaneously analyze multiple components of molecular and cellular events. Therefore, we expect that the 2nd-NIR fluorescence imaging using PbS/CdS QDs has great potential for the non-invasive imaging of dynamic

90 processes in biological systems *in vivo*.

References

1 R. Weissleder, *Nat. Biotechnol.*, 2001, **19**, 316-317.
100 2 J. V. Frangioni, *Curr. Opin. Chem. Biol.,* 2003, **7**, 626-634.
3 X. Gao, Y. Cui, R. M. Levenson, L. W. K. Chung and S. Nie, *Nat. Biotechnol.*, 2004, **22**, 969-976.

4 S. Kim, Y. T. Lim, E. G. Soltesz, A. M. D. Drand, J. Lee, A. Nakayama, J. A. Parker, T. Mihaljevic, R. G. Laurence, D. M. Dor, L. H. Cohn, M. G. Bawendi and J. V. Frangioni, *Nat. Biotechnol.*, 2004, **22**, 93-97.

5 X. Gao, L.Yang, J. A. Petros, F. F. Marshall, J. W. Simons and S. Nie, *Curr. Opin. Biotechnol.,* 2005, **16**, 63-72.

6 C. L. Amiot, S. Xu, S. Liang, L. Pan and J. X. Zhao, *Sensors,* 2008, **8**, 3082-3105.

7 A. M. Smith, M. C. Mancini and S. Nie, *Nat. Nanotechnol.*, 2009, **4**, 710-711.

8 Y. T. Lim, S. Kim, A. Nakayama, N. E. Scott, M. G. Bawendi and J. V. Frangioni, *Mol. Imaging*, 2003, **2**, 50-64.

9 L. A. Sordillo, Y. Pu, S. Pratavieira, Y. Budansky and R. R. Alfano, *J. Biomed. Opt.,* 2014, **19**, 056004.

10 M. J. O'Connell, S. M. Bachilo, C. B. Huffman, V. C. Moore, M. S. Strano, E. H. Haroz, K. L. Rialon, P. J. Boul, W. H. Noon, C. Kittrell, J. Ma, R. H. Hauge, R. B. Weisman and R. E. Smalley, *Science*, 2002, **297**, 593–596.

11 P. Cherukuri, S. M. Bachilo, S. H. Litovsky and R. B. Weisman, *J. Am. Chem. Soc.*, 2004, **126**, 15638–15639.

12 J. Lefebvre, D. G. Austing, J. Bond and P. Finnie, *Nano Lett.*, 2006, **6**, 1603–1608.

13 J. Crochet, M. Clemens and T. Hertel, *J. Am. Chem. Soc.*, 2007, **129**, 8058–8059.

14 T. K. Leeuw, R. M. Relth, R. A. Simonette, M. E. Harden, P. Cherukuri, D. A. Tsybouiski, K. M. Beckingham and R. B. Weisman, *Nano Lett.*, 2007, **7**, 2650–2654.

15 Z. Liu, W. Cai, L. He, N. Nakayama, K. Chen, X. Sun, X. Chen and H. Dai, *Nat. Nanotechnol.*, 2007, **2**, 47–52.

16 H. Jin, D. A. Heller and M. S. Strano, *Nano Lett.*, 2008, **8**, 1577–1585.

17 K. Welsher, Z. Liu, D. Daranciang and H. Dai, *Nano Lett.*, 2008, **8**, 586–590.

18 H. Jin, D. A. Heller, R. Sharma and M. S. Strano, *ACS Nano*, 2009, **3**, 149–158.

19 K. Welsher, Z. Liu, S. P. Sherlock, J. T. Robinson, Z. Chen, D. Daranciang and H. Dai, *Nat. Nanotechnol.*, 2009, **4**, 773–780.

20 K. Weisher, S. P. Sherlocka and H. Dai, *Proc. Natl. Acad. Sci. USA,* 2011, **108**, 8943-8948.

21 G. Hong, J. C. Lee, J. T. Robinson, U. Raaz, L. Xie, N. F. Huang, J. P. Cooke and H. Dai, *Nat. Med.*, 2012, **18**, 1841–1846.

22 H. Yi, D. Ghosh, M. H. Ham, J. Qi, P. W. Barone, M. S. Strano and A. M. Belcher, *Nano Lett.*, 2012, **12**, 1176–1183.

23 J. T. Robinson, G. Hong, Y. Liang, B. Zhang, O. K. Yaghi and H. Dai, *J. Am. Chem. Soc.*, 2012, **134**, 10664–10669.

24 Y. Du, B. Xu, T. Fu, M. Cai, F. Li, Y. Zhang and Q. Wang, *J. Am. Chem. Soc.*, 2010, **132**, 1470-1471.

25 P. Jiang, Z. Q. Tian, C. N. Zhu, Z. L. Zhang and D. W. Pang, *Chem. Mater.,* 2012, **24**, 3-5.

26 Y. Zhang, G. Hong, Y. Zhang, G. Chen, F. Li, H. Dai and Q. Wang, *ACS Nano*, 2012, **6**, 3695-3702.

27 P. Jiang, C. N. Zhu, Z. L. Zhang, Z. Q. Tian and D. W. Pang, *Biomaterials*, 2012, **33**, 5130-5135.

28 H. Y. Yang, Y. W. Zhao, Z. Y. Zhang, H. M. Xiong and S. N, Yu, *Nanotechnology*, 2013, **24**, 055706.

29 Y. Zhang, Y. Zhang, G. Hong, W. Hei, K. Zhou, K. Yang, F. Li, G. Chen, Z. Liu, H. Dai and Q. Wang, *Biomaterials*, 2013, **34**, 3639-3646.

30 Y. Zhang, Y. Liu, C. Li, X. Chen and Q. Wang, *J. Phys. Chem. C,* 2014, **118**, 4918-4923.

31 R. Gui, A. Wan, X. Liu, W. Yuan and H. Jin, *Nanoscale,* 2014, **6**, 5467-5473.

32 C. Li, Y. Zhang, M. Wang, Y. Zhang, G. Chen, L. Li, D. Wun and Q. Wang, *Biomaterials*, 2014, **35**, 393-400.

33 G. Chen, F. Tian, Y. Zhang, Y. Zhang, C. Li Q. Wang, *Adv. Func. Mater.,* 2014, **24**, 2481-2488.

34 J. M. Pietryga, D. J. Werder, D. J. Williams, J. L. Casson, R. D. Schaller, V. I. Kilimov and J. A. Hollingsworth, *J. Am. Chem. Soc.*, 2008, **130**, 4879-4885.

35 H. Zhao, D. Wang, T. Zhang, M. Chaker and D. Ma, *Chem Commun.*, 2010, **46**, 5301-5303.

36 M. S. Neo, N. Venkatram, G. S. Li, W. S. Chin and W. Ji, *J. Phys. Chem. C,* 2010, **114**, 18037-18044.

37 H. Zhao, M. Chaker, N. Wu and D. Ma, *J. Mater. Chem.,* 2011, **21**, 8898-8904.

38 H. Zhao, M. Chaker and D. Ma, *J. Mater. Chem.,* 2011, **21**, 17483-17491.

39 M. V. Kovalenko, R. D. Schaller, D. Jarzab, M. A. Loi and D. V. Talapin, *J. Am. Chem. Soc.*, 2012, **134**, 2457-2460.

40 Y. Justo, P. Geiregat, K. V. Hoecke, F. Vanhaecke, C. D. M. Donega and Z. Hens, *J. Phys. Chem. C,* 2013, **117**, 20171-20177.

41 F. Ren, H. Zhao, F. Vetrone and D. Ma, *Nanoscale,* 2013, **5**, 7800-7804.

42 M. A. Hines and G. D. Scholes, *Adv. Mater.,* 2003, **15**, 1844-1849.

43 L. Bakueva, I. Gorelikov, S. Musikhin, X. S. Zhao, E. H. Sargent and E. Kumacheva, *Adv. Mater.,* 2004, **16**, 926-929

44 S. Hinds, S. Myrskog, L. Levina, G. Koleilat, J. Yang, S. O. Kelly and E. H. Sargent, *J. Am. Chem. Soc.*, 2007, **129**, 7218-7219.

45 B. R. Hyun, H. Chen, D. A. Rey, F. W. Wise and C. A. Batt, *J. Phys. Chem. B,* 2007, **111**, 5726-5730.

46 K. A. Abel, J. Shan, J. C. Boyer, F. Harris and F. C. J. M. van Veggel, *Chem Mater.*, 2008, **20**, 3794-3796.

47 H. Zhao, M. Chaker and D. Ma, *J. Phys. Chem. C,* 2009, **113**, 6497-6504.

48 D. Wang, J. Qian, F. Cai, S. He, S. Han and Y. Mu, *Nanotechnology*, 2012, **23**, 245701.

49 J. Cao, H. Zhu, D. Deng, B. Xue, L. Tang, D. Mahounga, Z. Qian and Y. Gu, *J. Biomed. Mater. Res. Part A*, 2012, **100A**, 958-968.

50 Y. Nakane, Y. Tsukasaki, T. Sakata, H. Yasuda and T. Jin, *Chem Commun.*, 2013, **49**, 7584-7586.

51 T. Jin, F. Fujii, Y. Komai, J. Seki, A. Seiyama and Y. Yoshioka., *Int. J. Mol. Sci.*, 2008, **9**, 2044-2061.

52 Q. Ma, Y. Nakane, Y. Mori, M. Hasegawa, Y. Yoshioka, T. M. Watanabe, K. Gonda, N. Ohuchi and T. Jin, *Biomaterials*, 2012, **33**, 8486-8494.

53 M. Hasegawa, Y. Tsukasaki, T. Ohyanagi and T. Jin, *Chem. Commun.*, 2013, **49**. 228-230.

54 H. S. Choi, W. Liu, P. Misra, E. Tanaka, J. P. Zimmer, B. I. Ipe, M. G. Bawendi and J. V. Franginoi, *Nat. Biotechnol.*, 2007, **25**, 1165-1170.

55 X. Michalet, F. F. Pinaud, L. A. Bentolila, J. M. Tsay, S. Doose, J. J. Li, G. Sundaresan, A. M. Wu, S. S. Gambhir, S. Wiss, *Scinece*, 2005, **307**, 538-544.

56 M. A. Hines and P. Guyot-Sionnest, *J. Phys. Chem.*, 1996, **100**, 468-471.

57 B. O. Dabbousi, J. Rodriguez-Viejo. F. V. Mikulec, J. R. Heine, H. Mattoussi, R. Ober, K. F. Jensen and M. G. Bawendi, *J. Phys. Chem. B*, 1997, **101**, 9463-9475.

58 T. Jin, F. Fujii, E. Yamada, Y. Nodasaka and M. Kinjo, *J. Am. Chem. Soc.*, 2006, **128**, 9288-9289.

59 A. N. Bashkatov, E. A. Genia, V. I. Kochubey and V. V. Tuchin, *J. Phys. D: Apply. Phys.* 2005, **38**, 2543-2555.

60 Y. Iinuma, Y. Hirayama, N. Yokoyama, T. Otani, K. Nitta, H. Hashidate. M. Yoshida, H. Iida, D. Masui and S. Manabe, *J. Pediatr. Surg.,* 2013, **48**, 1123-1128.